Chemical Science

ROYAL SOCIETY OF CHEMISTRY

EDGE ARTICLE

View Article Online
View Journal

Cite this: DOI: 10.1039/d5sc04279h

All publication charges for this article have been paid for by the Royal Society of Chemistry

Received 11th June 2025
Accepted 15th September 2025

DOI: 10.1039/d5sc04279h

rsc.li/chemical-science

Bis-subporphyrin-like boron(III) complexes derived from indolo[2,3-*a*]carbazole-based cyclic bis-BODIPYs exhibiting persistent helical chirality

Aswini Spergen,[a] Pranav V. Bal,[a] Asif Khan Shameer Shameem,[a] Arun Joshy,[b] Anjana P. Nambiar,[a] Alex P. Andrews[a] and Gokulnath Sabapathi *[a]

Herein, we report the synthesis of 11,12-dihydroindolo[2,3-*a*]carbazole (InC) **1** incorporating expanded porphyrinoid **8**, and its boron(III) complexes (**8**·BF_2 and **8**·BF). These macrocycles exhibit a 'figure-eight' conformation that exists as a pair of helical enantiomers (*P*,*P* and *M*,*M*), confirmed by X-ray crystallographic analysis. The 'figure-eight' structures are stabilized by intramolecular hydrogen bonds such as NH···N and NH···F interactions. The synthesized macrocycles demonstrate excellent stability under ambient conditions. Further, the helically-locked structure **8**·BF exhibited closely held InC units with a distance of 6.17 Å and enabled facile optical resolution using chiral HPLC. Circular dichroism spectroscopy of enantiopure **8**·BF shows the Cotton effect at 692 nm extending to the near-IR region with $\Delta\varepsilon$ up to 150 M^{-1} cm^{-1}. The chiral induction of racemic macrocycle **8** was employed using enantiopure mandelic acids.

Introduction

Chirality in macrocyclic architectures has potential applications in enantioselective host–guest recognition, asymmetric catalysis, chiral sensing, and circularly polarized luminescence (CPL).[1–8] Expanded porphyrinoids are a unique class of functional macrocycles that exhibit intrinsic helical chirality owing to their twisted conformations, like 'figure-eight'[9,10] or 'Möbius bands'.[11–13] Such twisting arises from increased pyrrolic/heterocyclic units in the macrocyclic ring, which allows the conformational change from a planar to a distorted one.[14,15] However, obtaining a structurally-strained and rigid chiral framework to enable necessary chiral resolution is often challenging due to their intrinsic conformational flexibility. There are various strategies to achieve rigid 'figure-eight' conformations by overcoming the low racemization barriers through scaffold modification, strong intramolecular interactions, and metal coordination.[16–18] Recently, Latos-Grażynski and coworkers reported an intramolecular ring fusion of phenanthrene-incorporating hexaphyrin, leading to aza-helicenophyrin exhibiting helical chirality induced with conformational stability.[19] Very recently, our group disclosed an anthracene-based twisted cyclodipyrrin **2** with a 'figure-eight' conformation, stabilized by intramolecular hydrogen bonding interactions exhibiting CPL properties (Fig. 1).[20] At the same time, Lei and coworkers accomplished a configurationally locked pyrenidecaphyrin using palladium complexation, achieving near-IR chiroptical properties with a high absorption dissymmetry factor [$g_{abs} = 0.038$].[21] Subsequently, similar rigidification was achieved by BF_2 complexation, affording phenanthrene-based expanded porphyrinoid **3** with an increased racemization barrier.[22] Later, the flexible 'figure-eight' [38]octaphyrin was complexed with germanium, accomplishing the rigid bis-Ge(IV) complex **4**.[23]

In general, chiral induction in conformationally flexible macrocycles can be achieved through the introduction of a chiral guest such as amino acids, amines, *etc.*[24–26] This involves chirality transfer from the chiral guest to the achiral or racemic host macrocycles. In porphyrinoids, the amino nitrogen can be utilized for binding with the chiral acid guests.[27] In 2006, Setsune and coworkers employed this strategy on an octaphyrin to determine the absolute configuration of carboxylic acids. By introducing chiral guests, they successfully induced helical chirality in a racemic octaphyrin.[28]

Herein, we demonstrate the chiroptical properties of a rigid indolocarbazole-based expanded porphyrinoid *via* an unprecedented B–N bond formation. This work employs 11,12-dihydroindolo[2,3-*a*]carbazole **1** (InC) as a key precursor with a rigid and conjugated backbone possessing good solubility and stability.[29,30] It is recognized for its applications as a chemosensor and p-type semiconductor in developing OFET materials.[31–34] Doping boron into the molecular scaffold is an effective strategy due to the increased B–N bond stability, electron-deficient nature, altered HOMO–LUMO gaps, and redox behavior.[35–38] Seminal reports on organoborane macrocycles **5**

[a]*School of Chemistry, Indian Institute of Science Education and Research Thiruvananthapuram, Maruthamala PO, Kerala 695 551, India. E-mail: gokul@iisertvm.ac.in*

[b]*Organic Chemistry Division, National Chemical Laboratory, Pune 411008, India*

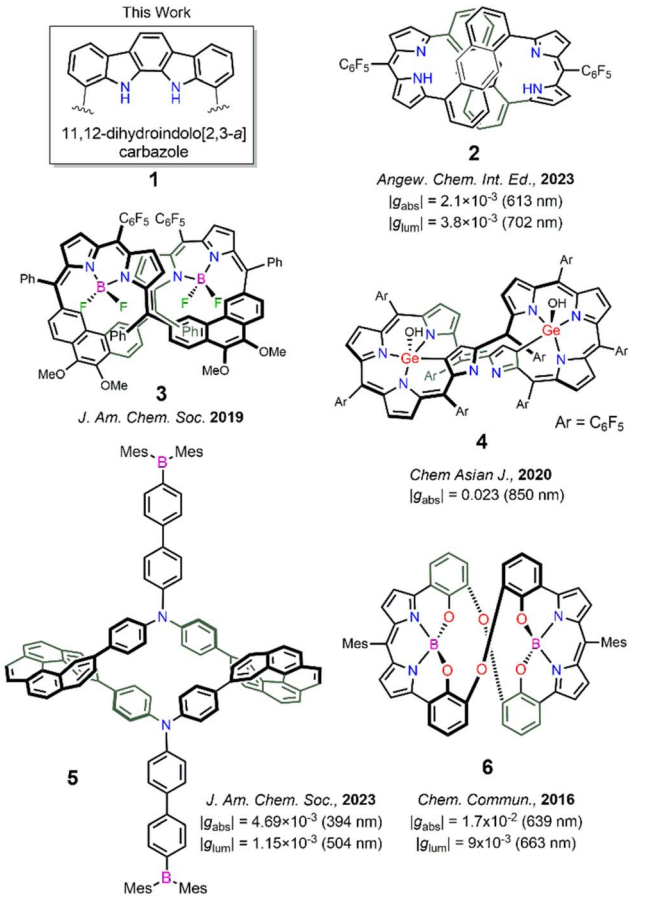

Fig. 1 Dihydroindolo(2,3-*a*)carbazole **1**, previously reported chiral porphyrinoid **2**, germanium and boron embedded macrocycles (**3** to **6**).

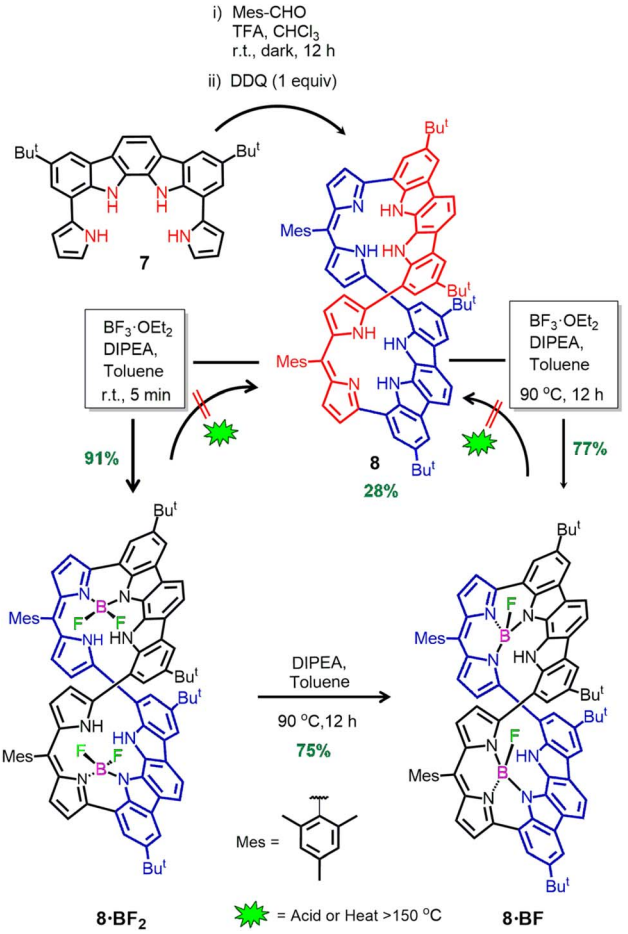

Scheme 1 Synthesis of macrocycle **8**, bis-BF_2 complex **8·BF$_2$**, and bis-BF complex **8·BF**. Bu^t = *tert*-butyl, TFA = trifluoroacetic acid, DDQ = 2,3-dichloro-5,6-dicyano-1,4-benzoquinone, DIPEA = diisopropylethylamine.

with enhanced CPL properties have emerged recently.[39–41] Additionally, the incorporation of the N_2O_2 boron moiety in the phenol-based macrocycle **6** exhibiting a helically locked conformation was reported by Nabeshima in 2016, which shows chiroptical responses in the near-IR region, with $|g_{lum}| = 9 \times 10^{-3}$.[42] Recently, our group reported a series of InC-embedded macrocycles, along with their mono-BODIPY complexes, exhibiting near-IR electrochromism.[43]

Results

Herein, we have utilized the key precursor **7** to accomplish the synthesis of the expanded porphyrinoid **8** (Scheme 1). Presumably, the presence of two distinct dipyrromethene moieties would allow BF_2 coordination on either macrocyclic pocket. However, facile BF_2 complexation at room temperature afforded **8·BF$_2$**. Further, the fused complex **8·BF** was obtained at higher temperature.

Synthesis

The synthesis began by treating the precursor **7** in the presence of trifluoroacetic acid with mesitaldehyde under dark conditions followed by oxidation with DDQ, resulting in the free macrocycle **8** (28%) (Scheme 1). Further, BF_2 complexation of **8** in the presence of DIPEA and $BF_3 \cdot OEt_2$ at room temperature in toluene instantly provided the bis-BF_2 complex (**8·BF$_2$**). The obtained **8·BF$_2$** was purified using flash silica column chromatography. To our surprise, the pyrrole fused product **8·BF** was obtained when **8·BF$_2$** was heated at 90 °C in toluene in the presence of DIPEA for 12 h. Alternatively, **8·BF** can also be obtained under typical BF_2 complexation by heating **8** at an increased temperature and extending the reaction time. The fused product **8·BF** was purified using neutral alumina column chromatography. The freebase **8** and its boron complexes (**8·BF$_2$** and **8·BF**) were found to be stable at room temperature for several days. They also show good solubility in common organic solvents. High-resolution mass spectral (HRMS) analysis revealed corresponding parent ion peaks at *m*/*z* values of 1253.6844 $[M + H]^+$ for **8**, 1348.6733 $[M]^+$ for **8·BF$_2$**, and 1308.6641 $[M]^+$ for **8·BF** (Fig. S1–S3). Surprisingly, treating with an acid such as CF_3COOH or heating the toluene solution of **8·BF** did not provide the free macrocycle, **8**. Further, **8·BF$_2$** under similar conditions did not revert to **8**, suggesting the structural stability of both **8·BF$_2$** and **8·BF**.

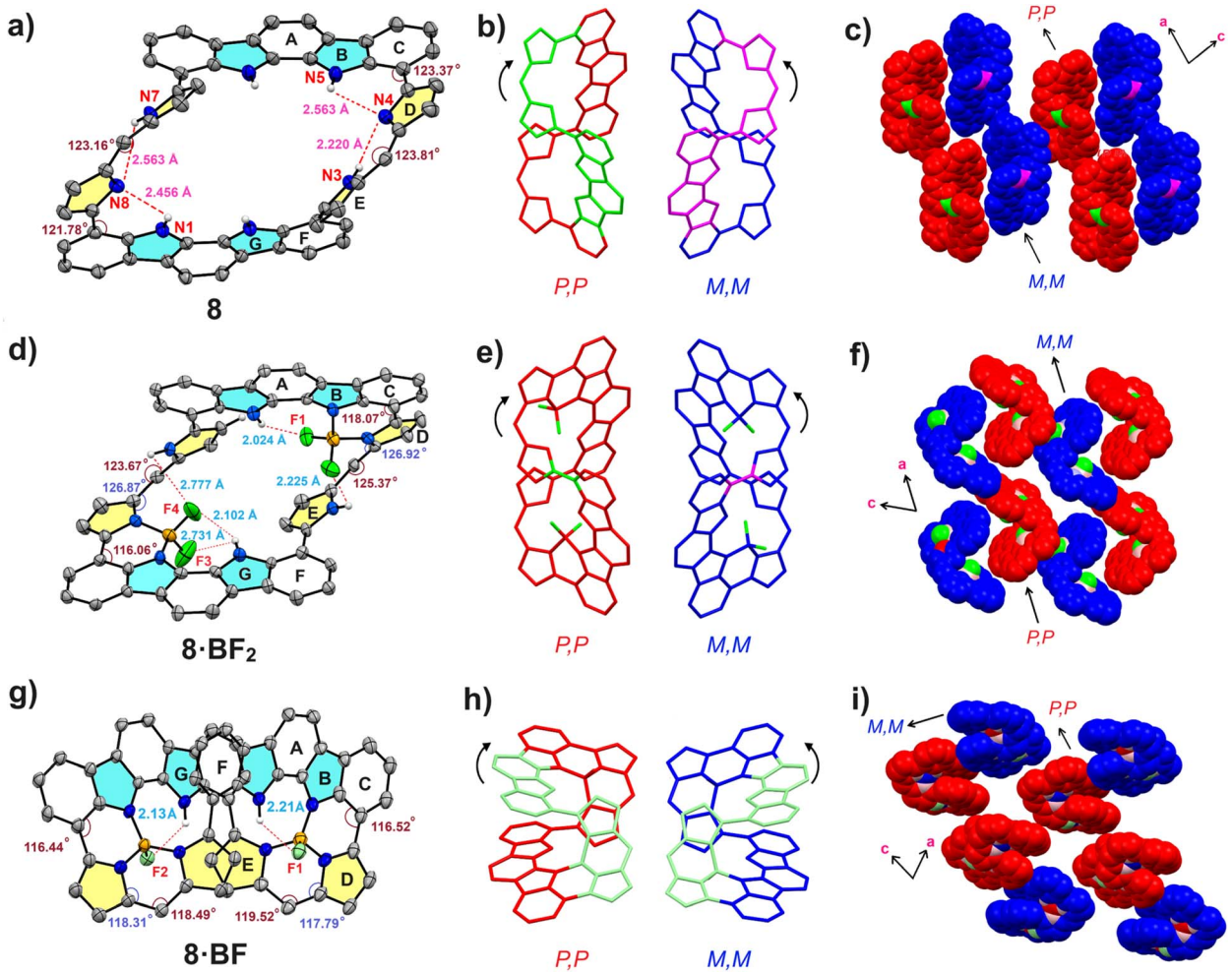

Fig. 2 (a, d and g) X-ray structures of **8**, **8**·BF_2, and **8**·**BF**. (b, e and h). *P*,*P* and *M*,*M* enantiomers of **8**, **8**·BF_2, and **8**·**BF**. (c, f and i) packing of enantiomers in **8**, **8**·BF_2, and **8**·**BF**. Meso and *tert*-butyl groups are omitted for clarity (ellipsoid probability level: 60%, grey—C, white—H, orange—boron, blue—N and light green—F).

Solution structure determination

The ^{1}H NMR spectra of macrocycles **8**, **8**·BF_2, and **8**·**BF** were recorded in $CDCl_3$. The ^{1}H NMR spectrum of **8** exhibits simple features, whereas **8**·BF_2 and **8**·**BF** show two set of signals, suggesting their asymmetry in solution upon boron complexation (Fig. S4a, S5a, and S6a). The pyrrolic-NH of **8** resonated as a broad singlet at 13.03 ppm due to NH tautomerism involving intramolecular hydrogen bonding. Meanwhile, four NHs from InC subunits appeared as a distinct singlet at 9.87 ppm. In **8**·BF_2, two macrocyclic pockets can be distinguished due to two sharp pyrrolic-NH signals at 11.06 and 11.02 ppm that do not exchange their sites. Further, there are only two NH signals from both InC subunits at 10.04 and 10.00 ppm, indicating that only one InC–NH is involved in BF_2-complexation. To our surprise, the solution structure of **8**·**BF** revealed only two NH signals corresponding to the InC ring (*ca.* 9.01 and 8.99 ppm), and no further NH signal was observed for the pyrrolic units, suggesting the fusion reaction occurred between the boron centre and pyrrolic nitrogen, similar to the bonding mode seen in B^{III}-subporphyrins.[44] However, the ^{11}B signal observed for **8**·**BF** is at 2.26 ppm (Fig. S8a), which is not in the shielded region as compared to the typical meso-triaryl subporphyrin B(III) complex exhibiting an upfield shifted signal at −15.1 ppm. This is due to the strong aromaticity of B(III) subporphyrins.[45] The difference in the fluorine environment is confirmed by the ^{19}F NMR spectrum, which exhibits two signals for **8**·BF_2 and one for **8**·**BF** (Fig. S7b and S8b).

X-ray crystallographic analysis

The solid-state structures of **8**, **8**·BF_2, and **8**·**BF** were unambiguously confirmed by X-ray diffraction analysis. Good quality crystals were obtained by slow vapor diffusion of methanol into an ethyl acetate solution of **8** and **8**·BF_2. Both were found to be crystallized in the triclinic system (space group: *P*1). On the contrary, crystals of **8**·**BF** were obtained from vapor diffusion of methanol into a dimethoxyethane solution, which crystallized in the monoclinic system (space group: *C*2/*c*). Further, *P*,*P* and *M*,*M* enantiomers of the three macrocycles were found equally in the crystal packing. Intriguingly, macrocycles **8** and **8**·BF_2 are packed as heterochiral chains of *P*,*P* and *M*,*M* enantiomers, which are stabilized through multiple intermolecular [CH···π] interactions, whereas **8**·**BF** is arranged as homochiral chains,

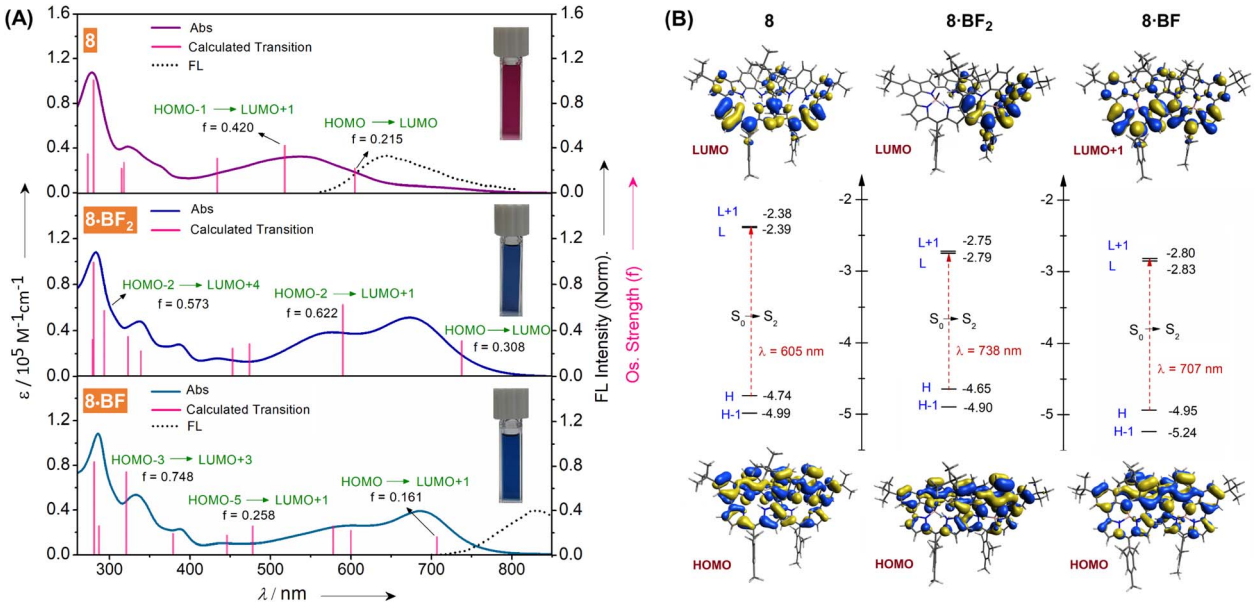

Fig. 3 (A) UV-visible absorption spectra of **8**, **8·BF$_2$**, and **8·BF** in CH_2Cl_2, along with their electronic transitions calculated using TD-DFT and emission spectra of **8** and **8·BF** in CH_2Cl_2. (B) Energy level diagrams of **8**, **8·BF$_2$** and **8·BF** with selected MOs calculated at the B3LYP/6-31G(d,p) level of theory.

governed by multiple intermolecular (π–π, CH···F and CH···π) interactions (Fig. S12–15). The 'figure-eight' conformations of all the macrocycles are deemed to be stabilized by multiple intramolecular hydrogen bonding interactions. In macrocycle **8**, four hydrogen bond interactions were observed: two between InC–NH (ring B) and pyrrole-N (ring D) (*ca.* 2.56 and 2.46 Å). Two more hydrogen bond interactions were observed between pyrrole-NH (ring E) and pyrrole-N (ring D) (*ca.* 2.56 and 2.22 Å) (Fig. 2).

Remarkably, in **8·BF$_2$**, the NH of InC (ring B) and the adjacent imino pyrrole (ring D) are involved in B–N bond formation, resulting in a *b*-annulated BF_2 complex without the involvement of the pyrrolic NH (ring E), confirming the acidic nature of the indolocarbazole-NH over pyrrolic NH. Further, the NH···F interactions between fluorine and NH of ring E could stabilize the helical conformation. In **8·BF**, the fluorine bound to each boron of the two macrocyclic pockets is stabilized with two intramolecular hydrogen bonding interactions between InC–NH (ring G; *ca.* 2.13 and 2.21 Å), with both fluorines in anti-arrangement. Notably, the boron in **8·BF$_2$** and **8·BF** adopts a nearly tetrahedral geometry. The crystal structure analysis also revealed that the distance between the two InC centroids of ring A in **8** and **8·BF$_2$** is measured to be 8.71 and 9.04 Å, respectively. However, the distance is significantly reduced in **8·BF** to 6.15 Å, indicating that the InC units are held closer, resulting in a more rigid 'figure-eight' structure upon fusion. Next, the bond angle between rings C and D gradually decreases upon boron complexation (*ca.* 121.78° in **8**; 116.06° in **8·BF$_2$**; and 115.81° in **8·BF**) suggesting the gaining of coplanarity between rings C and D. Similarly, the angle between rings D and E in **8** is smaller than **8·BF$_2$** (**8**: 123.81° and **8·BF$_2$**: 125.31°), whereas the angle in **8·BF** is further reduced to 119.52°. These subtle changes indicate that the steric congestion caused by BF_2 units resulted in a slightly enlarged cavity in **8·BF$_2$**, but ring fusion allowed **8·BF** to attain a rigid conformation with a decreased angle (Fig. S10–S12). The resulting fused bis-BF, *i.e.* tripyrrolylboron(III) macrocycle **8·BF**, demonstrates a BN_2F-type coordination, similar to the boron complexes of subporphyrins and subphthalocyanines.[44–48] This feature is similar to the BN_2OH coordination mode found in tripyrrolylboron(III) hexaphyrin reported by Osuka and coworkers in 2010.[49]

Optical and theoretical studies

The UV-Vis-NIR absorption spectrum of the freebase macrocycle **8** in CH_2Cl_2 exhibited a sharp band at 274 nm with a shoulder at 323 nm and a broad band reaching 537 nm (Fig. 3A). Meanwhile, **8·BF$_2$** displayed a greater bathochromic shift of the band at 536 nm to 674 nm, indicating the formation of the b-annulated BODIPY.[50–52] Further, the absorption spectral features of **8·BF** are similar to those of **8·BF$_2$**, with a slight difference in the overall features, suggesting a minimal change in the electronic structure (Fig. S17). The calculated optical energy gaps of the macrocycles reveal a decrease in the gap upon boron complexation (**8**: 1.85 eV; **8·BF$_2$**: 1.60 eV, and **8·BF**: 1.63 eV). Upon protonation, the lower energy band in **8** transformed into a broad band (λ_{max} = 651 nm) and a shoulder at 553 nm. Interestingly, the absorption features of protonated form **8·2H$^+$** with an optical band gap of 1.64 eV resemble the boron complexes **8·BF$_2$** and **8·BF** (Fig. S16). In addition, **8** and **8·BF** exhibit weak emission in the near-IR region upon excitation at 536 and 685 nm, respectively. Interestingly, they exhibit a Stokes shift of 3290 cm^{-1} for **8** and 2550 cm^{-1} for **8·BF** (Fig. S19). The absolute quantum yields of **8** and **8·BF** were calculated to be 1.34% and 0.09%, respectively (Fig. S21). However, the **8·BF$_2$** shows no emission, probably due to the pronounced spin–orbit

coupling and smaller singlet–triplet energy gaps as reported for benzo[*b*]-annulated BODIPYs.[53]

The computed absorption spectra of all the macrocycles agree with the experimental results, calculated using the CPCM solvation method at the B3LYP/6-31G(d,p) level of theory. For **8**, the lower energy absorption band at 536 nm is ascribed to the HOMO to LUMO and HOMO−1 to LUMO+1 transitions, whereas for **8·BF$_2$** the two transitions (HOMO to LUMO and HOMO−2 to LUMO+1) are related to the 652 nm absorption band (Fig. 3A). In **8·BF**, the absorption band at 685 nm originates from the HOMO to LUMO+1 transition. A reduction in the HOMO–LUMO band gap was observed for both BODIPYs as compared to **8** (**8**: 2.35 eV; **8·2H$^+$**: 1.96 eV; **8·BF$_2$**: 1.86 eV, and **8·BF**: 2.11 eV). The nucleus-independent chemical shift (NICS) values calculated for these macrocycles are close to "zero" (**8** = −0.08; **8·BF$_2$** = −0.14 and **8·BF** = +1.04), suggesting the absence of global conjugation (Fig. S33). Further, the non-aromaticity was supported by anisotropy of the current-induced density (ACID) plots, which show no continuous flow of magnetic vectors in the macrocycle, and the vectors move in a clockwise direction on the individual rings (Fig. S34).

Chiral separation and chiroptical properties

Macrocycles with 'figure-eight' conformation often exhibit helical or axial chirality depending on the symmetry. We initially attempted to separate the 'figure-eight' macrocycles (**8** and **8·BF$_2$**) using chiral HPLC, but could not achieve this after several attempts, presumably due to the fast interconversion between the *P*,*P* and *M*,*M* enantiomers. Interestingly, we were successful in performing chiral resolution of the helically locked 'figure-eight' macrocycle **8·BF**, using chiral stationary phase (JAIGEL-OA-4100-20, *n*-hexanes/THF = 80 : 20) (Fig. S23 and S24). The circular dichroism (CD) spectra of the two enantiomers of **8·BF** were recorded in CH_2Cl_2 and exhibited clear positive and negative Cotton effects (Fig. 4a). The absolute stereochemistry of the enantiomers was assigned based on the simulated CD spectra using TD-DFT calculations (Fig. 4a). Specifically, the *P*,*P* enantiomer showed a positive Cotton effect at 692 nm with $\Delta\varepsilon$ = 142.2 M^{-1} cm^{-1} and a negative Cotton effect at 346 nm ($\Delta\varepsilon$ = −62.5 M^{-1} cm^{-1}) and 289 nm ($\Delta\varepsilon$ = −151.1 M^{-1} cm^{-1}). For the *M*,*M* enantiomer, a negative Cotton effect is observed at λ/nm ($\Delta\varepsilon/M^{-1}$ cm^{-1}) of 692 nm (−149.9), and a positive Cotton effect at 346 nm (66.3) and 289 nm (142.3). The separated enantiomers of **8·BF** were dissolved in THF : *n*-hexane (1 : 1) and kept at room temperature for several days (>10 days), showing no sign of degradation or racemization, thus suggesting the robustness (Fig. S25). Furthermore, the enantiomers exhibited no racemization upon heating in toluene at 100 °C (Fig. S26). The maximum absorption dissymmetry factor $|g_{abs}|$ measured for **8·BF** is 0.0038 at 692 nm, 0.0014 at 346 nm, and 0.0015 at 289 nm (Table S2). The maximum CD response at 692 nm is correlated with S_0 to S_2 (HOMO to LUMO+1) transitions. It is well understood that a higher g_{abs} value can be

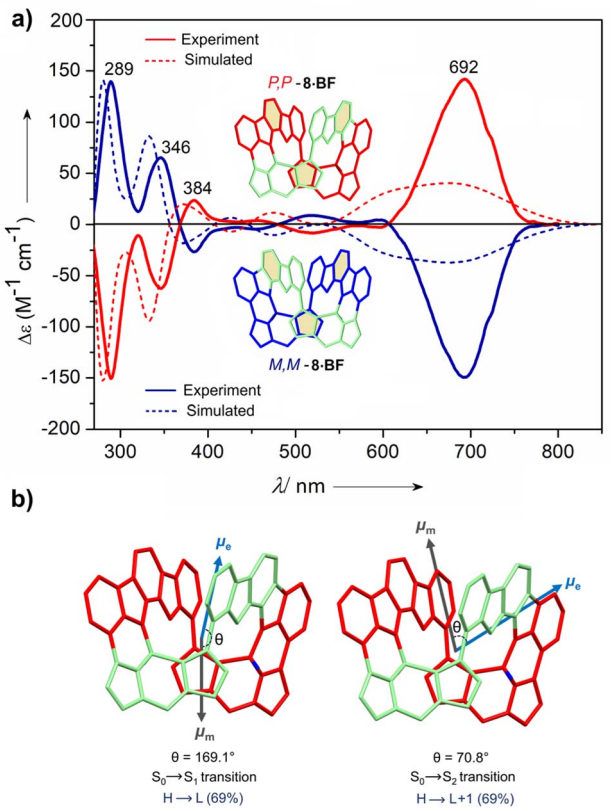

Fig. 4 (a) Experimental and simulated circular dichroism (CD) spectra for (*M*,*M*)-**8·BF** (blue, first fraction) and (*P*,*P*)-**8·BF** (red, second fraction) in CH_2Cl_2. (b) Angle between the transition dipole moments (μ_e and μ_m) at the B3LYP/6-31G(d,p) level of theory.

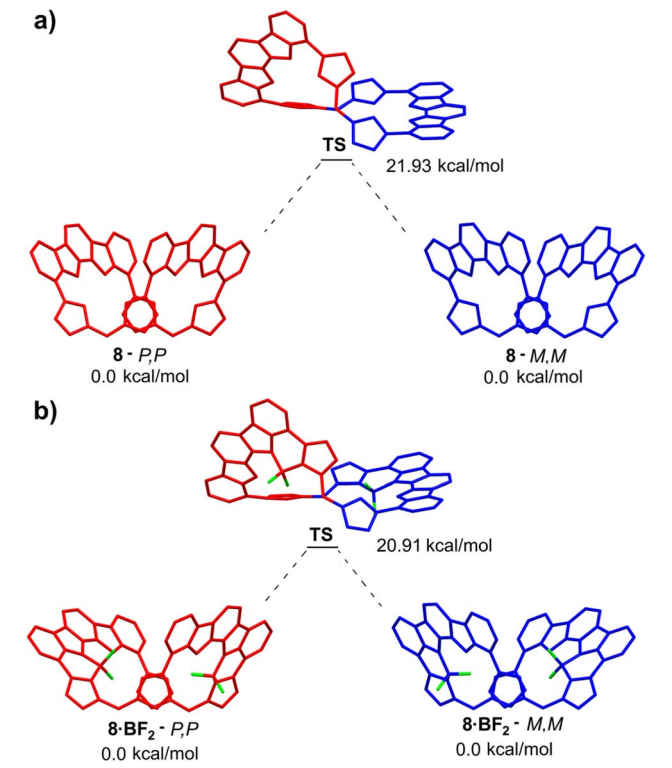

Fig. 5 Theoretical racemization barrier of (a) **8** and (b) **8·BF$_2$** calculated at the ωB97XD/6-31G(d,p) level of theory.

achieved only if the angle between the electric and magnetic transition dipole moments is either close to 0° or 180°.[54] In **8·BF**, although the S_0 to S_1 transition exhibits $\theta = 169.1°$ it does not contribute to the absorption at 692 nm whereas the S_0 to S_2 transition corresponding to absorption at 692 nm with $\theta = 70.8°$ provides a reasonable explanation for the lower $|g_{abs}|$ in the range of 10^{-3} (Fig. 4b). Unfortunately, no circularly polarized luminescence was observed for **8·BF**.

The theoretical racemization barrier of macrocycles **8** and **8·BF$_2$** was calculated at the ωB97XD/6-31G(d,p) level of theory (Fig. 5). It was found to be 21.93 and 20.91 kcal mol^{-1} at 298 K for **8** and **8·BF$_2$**, respectively. These barriers suggest that the enantiomers interconvert rapidly at room temperature, preventing chiral separation. In both macrocycles, the transition state corresponds to a half-twisted conformation. Further, we have attempted to induce the chirality by treating the racemic mixture of **8** with enantiopure mandelic acid and a-methoxyphenylacetic acid. To our surprise, a significant chiral response was achieved upon adding the acids (Fig. 6a and S30). In two separate experiments, upon the addition of D- or L-mandelic acid in dichloromethane, CD signals corresponding to *P*,*P* and *M*,*M* helices were observed, respectively. The CD responses are mirror images of each other. The CD signal intensity was increased upon increasing the equivalence of chiral mandelic acid (Fig. S27). Notably, a red-shifted CD signal was detected for the acid–base complexes of **8**, with the *P*,*P* helix exhibiting a positive Cotton effect and the *M*,*M* helix exhibiting a negative Cotton effect at 635 nm. These observations indicate a shift in the racemic equilibrium between the *P*,*P* and *M*,*M* conformers because of the chirality transfer from the point chirality of mandelic acid to the helical chirality of free macrocycle **8**. The temperature-dependent experiment of the host–guest complex showed a decrease in CD intensity upon increasing temperature, indicating a weakening of the interaction at higher temperatures (Fig. S28 and S29). In addition, the host–guest complex also does not exhibit the CPL activity. Further, the host–guest complex was optimised using DFT analysis, which exhibits intramolecular hydrogen bonding interactions between the macrocycle **8** and mandelic acids (Fig. 6b).

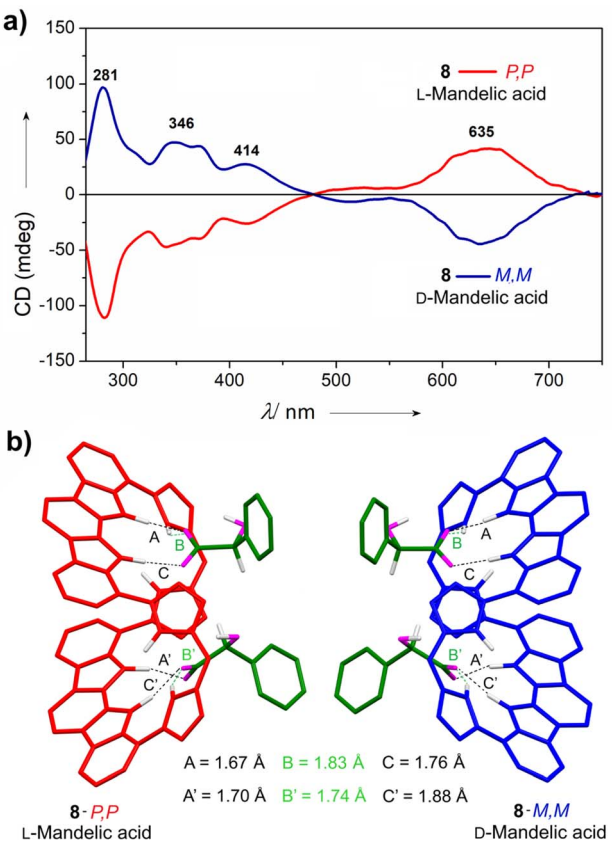

Fig. 6 (a) Chirality induction of **8** upon the addition of D- and L-Mandelic acid recorded in CH_2Cl_2 at 298 K, and (b) DFT optimized structures of *P*,*P* and *M*,*M* enantiomers of **8** with L- and D-mandelic acids, respectively.

Conclusions

In summary, we successfully synthesized the helically chiral expanded porphyrinoids containing dihydroindolo(2,3-*a*) carbazole, as evident from their crystal structures. The crystal structure of these 'figure-eight' macrocycles revealed the presence of both *P*,*P* and *M*,*M* enantiomers within the crystal packing. Hydrogen bonding interactions are deemed to stabilize these 'figure-eight' conformations, and further rigidification of the macrocycle was achieved through BF_2 complexation followed by a fusion reaction (**8·BF$_2$** → **8·BF**). Intriguingly, the absorption and emission spectra of **8·BF$_2$** and **8·BF** apparently reach towards the near-IR region (*ca.* 800 nm). Such a fusion reaction prevents the fast interconversion between *P*,*P* and *M*,*M* enantiomers of **8·BF**. Further, the rigid chiral framework of the **8·BF** complex facilitated the chiral resolution and afforded the stable enantiomers *P*,*P* and *M*,*M* with chiral response in the near-IR region with $\Delta\varepsilon$ of up to 150 M^{-1} cm^{-1} at $\lambda_{max} = 692$ nm. In order to achieve sterically-locked and conformationally-rigid macrocyclic systems, various strategies have been adopted.[18] Further, chiral induction of the conformationally flexible macrocycle **8** was performed with the enantiopure mandelic acids, giving a CD response of the mirror images. In this work, boron complexation (and B–N fusion) has proven to be an effective strategy to achieve a conformationally locked macrocycle. The chiral induction also has potential application in determining the absolute configuration of carboxylic acids.

Author contributions

Aswini Spergen – synthesis, characterisation, chiroptical studies, computational studies, manuscript writing; Pranav V. Bal – synthesis; Asif Khan Shameer Shameem - synthesis; Arun Joshy – chiral separation; Anjana P. Nambiar – chiroptical studies; Alex P. Andrews – single crystal diffraction and solving the X-ray data of all the macrocycles; Gokulnath Sabapathi – conceptualization, manuscript drafting and correction.

Conflicts of interest

There are no conflicts to declare.

Data availability

CCDC 2440526–2440528 (**8**, **8**·BF_2 and **8**·**BF**) contain the supplementary crystallographic data for this paper.[55a–c]

The experimental and theoretical data supporting this article have been included as part of the SI. Supplementary information: characterization data (HR-MS and NMR spectra), single-crystal X-ray analyses, absorption, fluorescence, chiroptical studies, and DFT calculations. See DOI: **https://doi.org/10.1039/d5sc04279h**.

Acknowledgements

S. G. thanks IISER Thiruvananthapuram for providing the facilities and ANRF (Formerly SERB) with Grant No. EEQ/2023/000756 for funding. A. S. thanks Prime Minister Research Fellowship from the Govt. of India.

Notes and references

1 T. Li, X. Zhu, G. Ouyang and M. Liu, *Mater. Chem. Front.*, 2023, **7**, 3879–3903.
2 M. J. Kim, Y. R. Choi, H. G. Jeon, P. Kang, M. G. Choi and K. S. Jeong, *Chem. Commun.*, 2013, **49**, 11412–11414.
3 J. Y. C. Lim, I. Marques, V. Félix and P. D. Beer, *J. Am. Chem. Soc.*, 2017, **139**, 12228–12239.
4 M. Dommaschk, J. Echavarren, D. A. Leigh, V. Marcos and T. A. Singleton, *Angew. Chem. Int. Ed.*, 2019, **58**, 14955–14958.
5 N. Pairault, H. Zhu, D. Jansen, A. Huber, C. G. Daniliuc, S. Grimme and J. Niemeyer, *Angew. Chem. Int. Ed.*, 2020, **59**, 5102–5107.
6 X. N. Han, Y. Han and C. F. Chen, *J. Am. Chem. Soc.*, 2020, **142**, 8262–8269.
7 X. Zhang, H. Liu, G. Zhuang, S. Yang and P. Du, *Nat. Commun.*, 2022, **13**, 1–10.
8 S. Tong, J. T. Li, D. D. Liang, Y. E. Zhang, Q. Y. Feng, X. Zhang, J. Zhu and M. X. Wang, *J. Am. Chem. Soc.*, 2020, **142**, 14432–14436.
9 E. Vogel, M. Broring, J. Fink, D. Rosen, H. Schmickler, J. Lex, K. W. K. Chan, Y. Wu, A. Dietmar, M. Nendel and K. N. Houk, *Angew. Chem. Int. Ed.*, 1995, **34**, 2511–2514.
10 A. Werner, M. Michels, L. Zander, J. Lex and E. Vogel, *Angew. Chem. Int. Ed.*, 1999, **38**, 3650–3653.
11 T. Tanaka, T. Sugita, S. Tokuji, S. Saito and A. Osuka, *Angew. Chem. Int. Ed.*, 2010, **49**, 6619–6621.
12 M. Izawa, T. Kim, S. I. Ishida, T. Tanaka, T. Mori, D. Kim and A. Osuka, *Angew. Chem. Int. Ed.*, 2017, **56**, 3982–3986.
13 R. Benchouaia, N. Cissé, B. Boitrel, M. Sollogoub, S. L. Gac and M. Ménand, *J. Am. Chem. Soc.*, 2019, **141**, 11583–11593.
14 M. Stępień, N. Sprutta and L. Latos-Grazyński, *Angew. Chem. Int. Ed.*, 2011, **50**, 4288–4340.
15 B. Szyszko, M. J. Biåek, E. Pacholska-Dudziak and L. Latos-Grazyński, *Chem. Rev.*, 2017, **117**, 2839–2909.
16 J. I. Setsune, A. Tsukajima, N. Okazaki, J. M. Lintuluoto and M. Lintuluoto, *Angew. Chem. Int. Ed.*, 2009, **48**, 771–775.
17 K. Mitsuno, T. Yoshino, I. Gupta, S. Mori, S. Karasawa, M. Ishida and H. Furuta, *Angew. Chem. Int. Ed.*, 2017, **56**, 14252–14256.
18 P. Han, M. Han, J. L. Sessler and C. Lei, *Chem. Eur. J.*, 2023, **29**, e20230305.
19 B. Szyszko, M. Przewoźnik, M. J. Białek, A. Białońska, P. J. Chmielewski, J. Cichos and L. Latos-Grażyński, *Angew. Chem. Int. Ed.*, 2018, **57**, 4030–4034.
20 A. Prasad Nambiar, P. Nag, R. Mariam Ipe, S. Reddy Vennapusa and S. Gokulnath, *Angew. Chem. Int. Ed.*, 2023, **62**, e202306566.
21 K. Liang, H. Chen, X. Wang, T. Lu, Z. Duan, J. L. Sessler and C. Lei, *Angew. Chem. Int. Ed.*, 2023, **62**, e202212770.
22 B. Szyszko, P. J. Chmielewski, M. Przewoźnik, M. J. Bialek, K. Kupietz, A. Bialońska and L. Latos-Grazyński, *J. Am. Chem. Soc.*, 2019, **141**, 6060–6072.
23 M. Izawa, T. Suito, S. ichiro Ishida, D. Shimizu, T. Tanaka, T. Mori and A. Osuka, *Chem. Asian J.*, 2020, **15**, 1440–1448.
24 S. Fa, K. Egami, K. Adachi, K. Kato and T. Ogoshi, *Angew. Chem. Int. Ed.*, 2020, **59**, 20353–20356.
25 H. Zhu, Q. Li, Z. Gao, H. Wang, B. Shi, Y. Wu, L. Shangguan, X. Hong, F. Wang and F. Huang, *Angew. Chem. Int. Ed.*, 2020, **59**, 10868–10872.
26 G. A. Hembury, V. V. Borokov and Y. Inoue, *Chem. Rev.*, 2008, **108**, 1.
27 J. I. Setsune, *J. Chem. Sci.*, 2012, **124**, 1151–1163.
28 J. M. Lintuluoto, K. Nakayama and J. I. Setsune, *Chem. Commun.*, 2006, 3492–3494.
29 T. Janosik, N. Wahlström and J. Bergman, *Tetrahedron*, 2008, **64**, 9159.
30 T. Janosik, A. Rannug, U. Rannug, N. Wahlström, J. Slätt and J. Bergman, *Chem. Rev.*, 2018, **118**, 9058.
31 K.-J. Chang, D. Moon, M. S. Lah and K.-S. Jeong, *Angew. Chem. Int. Ed.*, 2005, **44**, 7926–7929.
32 C. H. Lee, H. Yoon, P. Kim, S. Cho, D. Kim and W. D. Jang, *Chem. Commun.*, 2011, **47**, 4246–4248.
33 Y. Li, Y. Wu, S. Gardner and B. S. Ong, *Adv. Mater.*, 2005, **17**, 849.
34 C. H. Liu, M. R. Niazi and D. F. Perepichka, *Angew. Chem. Int. Ed.*, 2019, **58**, 17312–17321.
35 I. S. Yadav and R. Misra, *J. Mater. Chem. C*, 2023, **11**, 8688–8723.
36 Y. Wu, S. Li, H. Li, R. Ye and Z. Lu, *J. Mater. Chem. C*, 2023, **11**, 7144–7158.
37 Y. Qin, X. Liu, P. P. Jia, L. Xu and H. B. Yang, *Chem. Soc. Rev.*, 2020, **49**, 5678–5703.
38 Y. Adachi, T. Nabeya, K. Kawakami, K. Yamaji, F. Jäkle and J. Ohshita, *Chem. Eur. J.*, 2021, **27**, 3306–3314.
39 L. Menduti, C. Baldoli, S. Manetto, M. Bolte, H.-W. Lerner, G. Longhi, C. Villani, E. Licandro and M. Wagner, *Angew. Chem. Int. Ed.*, 2023, **62**, e20221546.
40 F. Zhao, J. Zhao, H. Liu, Y. Wang, J. Duan, C. Li, J. Di, N. Zhang, X. Zheng and P. Chen, *J. Am. Chem. Soc.*, 2023, **145**, 10092–10103.
41 J. F. Chen, X. Yin, B. Wang, K. Zhang, G. Meng, S. Zhang, Y. Shi, N. Wang, S. Wang and P. Chen, *Angew. Chem. Int. Ed.*, 2020, **59**, 11267–11272.

42 M. Saikawa, T. Nakamura, J. Uchida, M. Yamamura and T. Nabeshima, *Chem. Commun.*, 2016, **52**, 10727–10730.
43 A. Spergen, A. Kalaiselvan and S. Gokulnath, *Adv. Opt. Mater.*, 2023, **2300778**, 1–10.
44 C. G. Claessens, D. González-Rodríguez and T. Torres, *Chem. Rev.*, 2002, **102**, 835–853.
45 S. Hayashi, Y. Inokuma, S. Easwaramoorthi, K. S. Kim, D. Kim and A. Osuka, *Angew. Chem. Int. Ed.*, 2010, **49**, 321–324.
46 S. Shimizu, *Chem. Rev.*, 2017, **117**, 2730–2784.
47 A. Osuka, E. Tsurumaki and T. Tanaka, *Bull. Chem. Soc. Jpn.*, 2011, **84**, 679.
48 L. Liu, J. Kim, L. Xu, Y. Rao, M. Zhou, B. Yin, J. Oh, D. Kim, A. Osuka and J. Song, *Angew. Chem. Int. Ed.*, 2022, **61**, 1–5.
49 K. Moriya, S. Saito and A. Osuka, *Angew. Chem. Int. Ed.*, 2010, **49**, 4297–4300.
50 H. Lu, J. MacK, Y. Yang and Z. Shen, *Chem. Soc. Rev.*, 2014, **43**, 4778–4823.
51 Y. Ni, W. Zeng, K. W. Huang and J. Wu, *Chem. Commun.*, 2013, **49**, 1217–1219.
52 A. Wakamiya, T. Murakami and S. Yamaguchi, *Chem. Sci.*, 2013, **4**, 1002–1007.
53 N. Xu, Y. Xiao, Z. Ni, L. Gai, Z. Zhou and H. Lu, *Phys. Chem. Chem. Phys.*, 2021, **23**, 17402–17407.
54 W. Fan, T. M. Fukunaga, S. Wu, Y. Han, Q. Zhou, J. Wang, Z. Li, X. Hou, H. Wei, Y. Ni, H. Isobe and J. Wu, *Nat. Synth.*, 2023, **2**, 880–887.
55 (*a*) A. Spergen, P. V. Bal, S. S. Asif Khan, A. Joshy, A. P. Nambiar, A. P. Andrews and G. Sabapathi, CCDC 2440526: Experimental Crystal Structure Determination, 2025, DOI: **10.5517/ccdc.csd.cc2mxkns**; (*b*) A. Spergen, P. V. Bal, S. S. Asif Khan, A. Joshy, A. P. Nambiar, A. P. Andrews and G. Sabapathi, CCDC 2440527: Experimental Crystal Structure Determination, 2025, DOI: **10.5517/ccdc.csd.cc2mxkpt**; (*c*) A. Spergen, P. V. Bal, S. S. Asif Khan, A. Joshy, A. P. Nambiar, A. P. Andrews and G. Sabapathi, CCDC 2440528: Experimental Crystal Structure Determination, 2025, DOI: **10.5517/ccdc.csd.cc2mxkqv**.